Heat Transfer Enhancement in a Receiver Tube of Solar Collector Using Various Materials and Nanofluids

Djemaa Guerraiche
Applied Energy Physics Laboratory (LPEA)
Department of Physics
Faculty of Matter Sciences
University of Batna 1
Batna, Algeria
d.guerraiche@gmail.com

Khelifa Guerraiche
Mechanical Engineering Department
Faculty of Technology
University of Batna 2
Batna, Algeria
guer.khelifa@yahoo.com

Zied Driss
Laboratory of Electromechanical Systems (LASEM)
National School of Engineers of Sfax (ENIS)
University of Sfax, Sfax, Tunisia
zied.driss@enis.tn

Atef Chibani
Department of Chemical Engineering
University Salah Boubnider Constantine 3
Constantine, Algeria
chibaniatef@gmail.com

Slimane Merouani
Department of Chemical Engineering
University Salah Boubnider Constantine 3
Constantine, Algeria
s.merouani@yahoo.fr

Cherif Bougriou
Mechanical Engineering Department
Faculty of Technology, University of Batna 2
Batna, Algeria
c.bougriou@univ-batna2.dz

Received: 21 July 2022 | Revised: 5 August 2022 | Accepted: 8 August 2022

Abstract-The solar flux distribution on the Parabolic Trough Collector (PTC) absorber tube is extremely non-uniform, which causes non-uniform temperature distribution outside the absorber tube. Therefore, it generates high thermal stress which causes creep and fatigue damage. This presents a challenge to the efficiency and reliability of parabolic trough receivers. To override this problem, we have to homogenize the heat flux distribution and enhance the heat transfer in the receiver's absorber tube to improve the performance of the PTC. In this work, 3D thermal and thermal stress analyses of PTC receiver performance were investigated with a combination of Monte Carlo Ray-Trace (MCRT), Computational Fluid Dynamics (CFD) analysis, and thermal stress analysis using the static structural module of ANSYS. At first, we studied the effect of the receiver tube material (aluminium, copper, and stainless steel) on heat transfer. The temperature gradients and the thermal stresses were compared. Second, we studied the effect of the addition of nanoparticles on the working Heat Transfer Fluid (HTF), employing an Al_2O_3-H_2O based nanofluid at various volume concentrations. To improve the thermal performance of the PTC, a nanoparticle volume concentration ratio of 1%–6% is required. The results show that the temperature gradients and thermal stresses of stainless steel are significantly higher than those of aluminium and copper. From the standpoint of thermal stress, copper is recommended as the tube receiver material. Using Al_2O_3 in water as an HTF increases the average output temperature by 2%, 6%, and 10% under volume concentrations of 0%, 2%, and 6% respectively. The study concluded that the thermal efficiency increases from 3% to 14% for nanoparticle volume fractions ranging from 2% to 6%.

Keywords-heat transfer; nanofluids; solar concentrator; receiver; non-uniform heat flux; temperature gradients

I. INTRODUCTION

The use of renewable energies has become essential to the reduction of the consumption of fossil resources and the production of carbon dioxide (CO_2), which is the main gas responsible for the greenhouse effect. The technology of Concentrated Solar Power (CSP) can meet the demands for thermal and electrical energy. The benefits of using a CSP technology with a PTC system are: it is best suited for a wide range of industrial applications and can contribute to thermal energy production, which can have significant economic, environmental, and social implications [1]. Recently, the PTC has been developing towards a higher concentration ratio and operating temperature for the purposes of reducing the

Corresponding author: Djemaa Guerraiche

investment cost and improving its thermal efficiency, especially at high temperatures. This is an important goal in order for these technologies to be energetically and financially viable [2]. However, the PTC suffers from several problems and failures, especially concentrated solar Non-Uniform Heat Flux (NUHF) distribution on the outer surface of the absorber tube. In addition, the heat flux is small near the top wall where the collimated energy is incident and is large near the bottom wall [3]. NUHF causes high local temperature and big temperature gradient in solar receivers due to the restricted thermal conductivity of the receiver tube and the thermal convection capacity inside the tube, producing an increase in thermal stress. This causes the absorber tube to deviate from the focal plane and large increase in optical losses because the selective coating degrades when the local temperature is too high, limiting the maximum working temperature. All these issues represent challenges that will have a long-term impact on the PTC's efficiency and safety [4]. Authors in [5] discovered that the maximum temperature differential for safe functioning of receiver tubes is around 50K. Furthermore, strong temperature gradients have many repercussions circumferentially, which may be summed by the deflection of the absorber tube. This causes the absorber tube to deviate from the concentrator's focus line, causing optical loss. When the local temperature is too high, the selective coating degrades, limiting the maximum operating temperature. As a result of the thermal breakdown of the HTF, hydrogen production and penetration occur [6], resulting in increasing heat loss, material degradation, heat stress, and deformation of the absorber tube. These pose significant obstacles to the concentrated solar system's safe and efficient functioning. To solve this issue, we must homogenize the heat flow distribution by flattening the temperature distribution, lowering the peak temperature and the temperature gradient. Recent studies have concentrated on improving thermal transfer and thermal distribution uniformity. A simple solution to flattening the temperature distribution is to homogenize the flow distribution. Heat transfer enhancement technology can reduce thermal losses and thermal stress while increasing heat transfer rates between the absorber tube and HTF at a low cost. The solutions can be roughly classified into three groups: Improvements to the tube's thermal conductivity, collector optimization to homogenize solar energy, and augmentation of convective heat transfer within the absorber tube [7].

Receiver tubes are subjected to a harsh operating environment. To alleviate the extreme operating conditions and ensure the receiver's durability, dependability, and integrity throughout its lifecycle, special consideration was required when selecting the receiver material. High corrosion resistance, optimal physical and mechanical properties, excellent fabricability, and a higher capacity for flux density are all critical criteria. Several solutions have been adopted by enhancing the thermal conductivity of the absorber tube and employing an absorber with thermal compensator and heat transfer improvement techniques [8]. Using selective materials, solution techniques aimed to improve the thermal conductivity of the absorber tube have been proposed for the PTC receiver. Authors in [9] conducted a structural and thermal analysis of a PTC absorber tube to investigate the effect of material variations on temperature distribution flattening. Steel, copper, aluminium, and bimetallic materials (Cu-Fe) have been investigated. They concluded that when using copper, the circumferential temperature non-uniformity was less bending due to less thermal load than using steel. Using a bimetallic tube improves temperature distribution and reduces maximum deflection by 45–49%. Authors in [2] presented an experimental investigation in which the steel tube was replaced with a copper tube. The reduced bending of the absorber tube was caused by the lower circumferential temperature variations due to copper's strong thermal conductivity.

II. HOMOGENIZING SOLAR FLUX DISTRIBUTION

A more straightforward way to flatten the temperature distribution appears to be the homogenization of the flux distribution. Several researchers proposed innovative concentrators for flux homogenization. The heat flow gradient in the absorber tube must be reduced and homogenized. Authors in [10] proposed improvements based on the conventional PTC and a secondary reflector was added overhead the tube. The numerical results showed that the heat flux gradient was reduced by 70.37%, and the temperature gradient from 159.39K to 24.16K. Authors in [11] used a variable focus PTC, in which the focal length varied as a function of the reflector's motion relative to the receiver, significantly enhanced the flux distribution's homogeneity. Authors in [12] placed a secondary reflector within the annular gap in order to reflect more sun rays onto the top of the absorber. Authors in [13] investigated the heat flux distribution on the outside surface of the PTC absorber tube in order to lower the tube's temperature gradient by relocating the absorber tube away from the focal line and toward the parabola and adding a secondary reflector. The results show that installing another reflector overhead the absorber tube improves the heat flux distribution and reduces heat flux gradient by 70.37%.

III. HEAT TRANSFER ENHANCEMENT AND OPTIMIZATION

Heat transfer improvement might result in a more uniform temperature distribution in the metal tube, reducing thermal deformation in the receiving tube. For the PTC receiver, a number of strategies for enhancing convective heat transfer have been proposed. Authors in [14] used an absorber with a thermal compensator at the parabolic dish concentrated solar receiver, which contains a Phase Change Material (PCM) to produce uniform heat distribution. Thermal performance is improved by using PCMs as thermal energy storage. Homogeneous temperature distribution was observed on the PCM integrated receiver in the absence of solar radiation. A non-uniform temperature distribution was discovered during the charging of the PCM included within the solar receiver. Authors in [15] presented a novel PTC receiver design based on a concentric absorber tube filled with PCM. The absorber was regarded as a component of transitory thermal heat storage. The results validated the suggested design and verified that combining PTC and PCM in the receiver peripheral can improve the thermal performance of the provided system. In [16], for solar cascade heat collection, a new PTC with a concentric receiver tube based on two HTFs, Syltherm-800 oil, was presented. The findings revealed that the absorber tube's peak temperature and circumferential temperature gradient

were lower than regular PTC at the same mass flow rate. The absorber tube's maximum temperature and temperature difference lowered to 66K and 65K respectively. For the PTC receiver, several strategies for improving convective heat transfer have been proposed. This technology employs helical swirl generators, treated areas, vortex generators, displacement increase devices, extended surfaces, jagged surfaces, and nanoparticles [17]. According to these studies, the peak temperature and temperature gradient can be minimized. In [18], the impact of swirl inserts with and without nanofluids on PTCs with non-uniform heating flux was examined. The results showed that combining the swirl inserts and nanofluids improved the Nusselt number by 57.4% while the maximum reduction in thermal losses was 23%. The Nusselt number, on the other hand, was enhanced by 15.57% when utilizing nanofluid only.

The working fluid is one of the most important components of a solar receiver since it plays an important role in heat transmission. During the last 25 years, nanotechnology has found applications in solar energy production. The use of nanofuids has transformed material science, and they have been used as potential alternative fluid solutions for increasing the efficiency and profitability of thermal systems. Adding nanoparticles to the heating fluid presents the best solution to improve thermal conductivity and thermo-physical and heat transfer properties of the fluid [19]. In fact, nanofluids have a favorable effect on the performance of the PTC. The heat transfer performance obtainable with nanofluids is known to surpass the performance of heat transfer liquids available today [20]. The most used nanofluids contain nanoparticles such as Al, Fe_2O_3, Al_2O_3, Cu, TiO_2, and SiO_2 [21]. Some studies on the use of nanofluids for solar energy harvesting are available in the literature. For example, authors in [22] investigated the application of nanofluids in concentrating a solar PTC. The effect of several nanofluids employed as working fluid on the performance of solar thermal collectors was studied experimentally. Authors in [23] discussed the progressive application of nanofluids in solar collectors with different thermophysical properties. In addition, they evaluated the performance of different types of solar collectors. Authors in [24] proposed a mathematical model for the investigation of the effect of nanofluid concentration on PTC. They found that using nanofluids in a PTC improves its thermal efficiency. Authors in [25] presented an experimental study of the heat transfer and friction factor of silver nanofluids in a PTC receiver with twisted tape inserts. They confirmed that using nanofluids increases the heat transfer performance of the receiver. Authors in [26] confirmed that the performance of concentrating solar thermal systems with a nanofluid as working fluid has an excellent potential for power tower applications improving efficiency by 5%–10%. Authors in [27] investigated the performance of nanofluids on PTC systems and improved the efficiency by at least 5% [27]. Authors in [28] presented an experimental study to evaluate the thermal efficiency of a PTC using nanoparticles of alumina (Al_2O_3) in water with a volume fraction of 1% and 3% as HTF. The results showed that with nanofluid as working fluid, the maximum efficiencies were 52.4% and 57.7%, while for water, these efficiencies were 40.8% and 46.5% for 3% and 1% volume fraction respectively. PTC thermal enhancement has recently attracted considerable attention. The enhancement of PTC performance can be achieved by modifying the material, modifying the geometry, and using nanofluids instead of conventional base fluids. Even so, utilizing nanofluids on PTCs provided a positive result. These results are still facing several breaking points in the method of using a HTF [29]. Finding the optimal configuration of various parameters, such as receiver formation and geometry, receiver size and material, HTF, and regulation of the maximum heat flow, is one of the most challenging and important research purposes for enhanced thermal systems to further improve efficiency and profitability through innovation in design and application of new fluids and new materials.

This work presents a three-dimensional numerical study of the thermal and thermal stress performance of a PTC. In order to attain this goal, the suggested approach consists of two main steps. The impact of the absorber tube material on heat transmission was investigated in the first step. The performance of PTC receivers was studied using a combination of Monte Carlo Ray-Trace (MCRT), Computational Fluid Dynamics (CFD) simulation using Ansys Fluent software, and thermal stress analysis using ANSYS' static structural module. We will solve the temperature distributions in the heat transfer analysis, and the thermal stress analysis will use the interpolated temperature distributions specified at the nodes of the CFD meshes as input data for the nodes. A comparative study of numerous materials, such as copper, aluminum, and stainless steel, is employed and compared to find which is ideal for a small-sized PTC under actual NUHF. Second, the effect of the addition of nanoparticles on the working fluid, employing Al_2O_3-H_2O based nanofluid at various volume concentrations is carried out. The computational model is developed in Ansys Fluent environment.

IV. PHYSICAL MODEL

Figure 1 shows the physical model considered in this work. The PTC system consists of a mirror folded into a parabolic shape with a heat collecting element at its focus. In the numerical study, the rim angle (φ_r) of the collector is 90° and the total aperture area (Ap = W×L) is 1.80m^2. The receiver of the parabolic trough solar collector consists of a metallic tube that is enclosed in a glass envelope. The absorber tube is coated with a selective coating that has a high absorptivity of the incoming solar radiation and a low emissivity of infrared radiation. The geometrical dimensions and optical properties of the PTC system are defined in Table I. In this work, a three-dimensional analysis of the thermal losses and thermal stress performance of a solar PTC receiver was investigated through studying the influence of the receiver tube, material type, and the nanofluid used as the working fluid. To improve the thermal performance of the PTC and homogenize the flux distribution for flattening the temperature distribution, various types of materials were used for the receiver heat transfer enhancement, namely copper, stainless steel, aluminium, and water containing nanoparticles of Al_2O_3. 321H stainless steel was used for the absorber tube due to its low bending behavior and high strength capability [30]. The thermal properties of absorber materials are given in Table II. In these conditions, the

concentration ratio and the mass flow rate are equal to 0%–6% and 0.005kg/s respectively. For our analysis, the solar collector shown in Figure 2 was chosen as the geometrical model in the simulations.

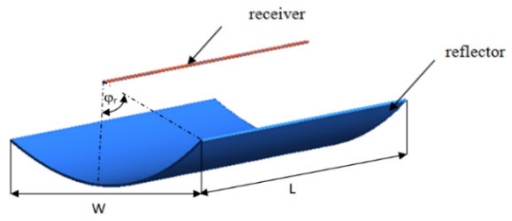

Fig. 1. View of the parabolic trough collector and its components.

TABLE I. GEOMETRICAL PARAMETERS OF THE PTC [15]

Receiver tube	
Inner diameter of receiver tube	0.027 m
Outer diameter of receiver tube	0.028 m
Inner diameter of pyrex cover	0.048 m
Outer diameter of pyrex cover	0.050 m
Collector	
Focal length, f	0.25 m
Aperture width, w	1.0 m
Rim angle, φ_r	90°
Length, L	1.80 m
Geometrical concentration ratio, C	13
Mirrors reflectivity, ρ	0.91
Slope error σ_{slope}	2 mrad
Specularity error σ_{spec}	2 mrad

TABLE II. STEEL, ALUMINA, AND COPPER ABSORBER TUBE PHYSICALS PARAMETERS [30]

Parameter	**321H Stainless steel**	**Alumina**	**Copper**
Density (kg.m^{-3})	8030	3850	8978
Conductivity (W.m-1.K^{-1})	17.3	36	387.6
Specific heat (J.kg-1.K^{-1})	512	773	381

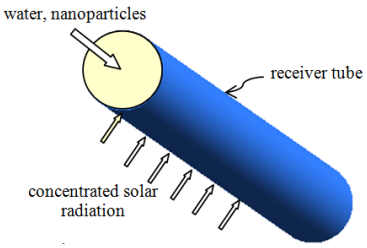

Fig. 2. Receiver parabolic trough solar collector geometry.

V. NUMERICAL MODEL AND MATHEMATICAL FORMULATION

A three-dimensional optic-thermal coupling model is used to analyze the heat transfer process in a PTC system employing Al_2O_3/water nanofluid as the HTF. The Monte Carlo Ray Trace (MCRT) code is used to calculate a realistic non-uniform solar radiation heat flux distribution on the outside wall of the absorber tube to expose the optical features of the proposed PTC system. The solar flux distribution created using the MCRT approach was regarded as heat flux boundary conditions in the steady state heat transfer investigation for CFD analysis. In the estimation of heat flux distributions, actual variables such as sun shape, incidence angle, optical characteristics, and numerous optical defects, were taken into consideration. The expected Direct Normal Irradiance (DNI) was 1000W/m^2. The thermal performance of the PTC was studied utilizing a Computational Fluid Dynamics (CFD) software tool and a nanofluid as the working fluid. The Reynolds averaged Navier-Stokes equations were solved using the finite volume approach in the commercial computational fluid dynamics package Ansys Fluent 16.0. The finite volume approach was used to discretize the governing equations of continuity, nanoparticle conservation, momentum, and energy. The convective and diffusive components in momentum and energy equations were discretized using the second-order upwind approach. For pressure discretization, the PRESTO scheme was utilized. The SIMPLE method was used to solve the velocity pressure coupling problem. Nanofluid flow modeling is classified into two categories: the single-phase flow in which the base fluid and the suspended nanoparticles are assumed homogenous, taking into consideration the thermal characteristics of the nanofluid and relying on published correlations, and two-phase flow which separates the base fluid from the suspended nanoparticles. FLUENT supports three models: Volume Of Fluid (VOF), mixed, and Eulerian. The single-phase method was utilized in this study, which is regarded as an accurate method when the nanoparticle concentration and diameter are less than 10% and 100nm respectively. [31].

VI. MESH INDEPENDENCE VERIFICATION

A three-dimensional geometry was created, and a tetrahedral mesh was placed over the absorber tube's fluid domain. Figure 3 depicts the absorber tube's mesh geometry. A grid independence test was performed to ensure that the mesh value is not affected by the grid. Table III shows the results of the mesh sensitivity study for the output temperature of a working fluid.

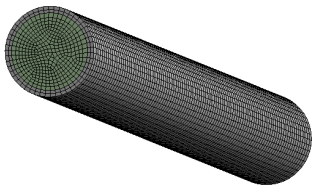

Fig. 3. 3D meshing of the absorber tube.

TABLE III. GRID INDEPENDENCE STUDY

Grid	**Outlet temperature (K)**
182680	328.12
256660	327.55
365760	326.51
406460	326.50

VII. HEAT TRANSFER FLUID PROPERTIES

Water with Al_2O_3, a frequently used and affordable nanoparticle, was employed as the base fluid in this study. The nanofluids' qualities are determined by the thermophysical parameters of the base fluid, the volume concentration ratio of

nanoparticles, and the temperature. Table IV lists the characteristics of Al_2O_3 nanoparticles [32].

TABLE IV. PROPERTIES OF THE Al_2O_3 NANOPARTICLES

	Density ($kg.m^{-3}$)	**Conductivity ($W.m\text{-}1.K^{-1}$)**	**Specific heat ($J.kg\text{-}1.K^{-1}$)**
Al_2O_3	3850	36	773

Nanofuid density, heat capacitance, dynamic viscosity, and thermal conductivity are determined from the following equations [33]. The density of the nanofluid is determined by:

$$\rho_{nf} = (1\text{-}f)\rho_f + f\,\rho_p \quad (1)$$

where ρ, f, p, nf and ϕ denote the density, base fluid, nanoparticle, and nanofluid and the volumetric concentration of Al_2O_3 in the base fluid respectively. The ratio between the thermal conductivities of the nanofluid K and the base fluid K_f is defined as follows:

$$\frac{K}{K_f} = \frac{\tau + (\eta - 1) - (\eta - 1)(1 - \tau)\phi}{\tau + (\eta - 1) + (1 - \tau)\phi} \quad (2)$$

The ratio between the thermal conductivities of the particles K_p and the base fluid is defined as:

$$\tau = K_p / K_f \quad (3)$$

The aspect ratio is given by (4), where ξ is the sphericity:

$$\eta = \xi/3 \quad (4)$$

The viscosity of the nanofluid is defined by:

$$\frac{\mu_{nf}}{\eta_{bf}} = 1 + 2{,}5\phi \quad (5)$$

The specific heat of the nanofluid is given by:

$$Cp_{nf} = (1-\phi)Cp_f + \phi\, Cp_p \quad (6)$$

VIII. THERMAL PERFORMANCE

The thermal efficiency η_{th} of the PTC system is determined as follows:

$$\eta_{th} = \frac{Q_U}{Q_S} \quad (7)$$

where Q_U is the useful gained thermal energy and Q_s is the available solar energy:

$$Q_s = A_a \times I_b \quad (8)$$

where A_a is the the aperture area of the solar collector:

$$A_a = w \times L \quad (9)$$

The useful gained thermal energy Q_u is determined based on the mass flow rate of the HTF, mass flow rate, and the fluid temperatures at the inlet and outlet, T_{in} and T_{out} [34]:

$$Q_u = \dot{m}\, Cp(T_{out} - T_{in}) \quad (10)$$

where $\dot{m}$, C_p, T_{out}, and T_{in} are the mass flow rate, specific heat capacity, and inlet and outlet heat transfer fluid temperature.

The conventional definition of the local convective heat transfer coefficient can be calculated in terms of the inner wall temperature of the absorber tube T_w, surface heat flux q", and the average temperature T_{ave} of the inlet and the outlet:

$$h_f = \frac{q''}{(T_w - T_{ave})} \quad (11)$$

IX. HYDRAULIC PERFORMANCE

The pressure drop in the solar absorber tube can be determined as follows [35]:

$$\Delta P = P_{av,inl} - P_{av,out} \quad (12)$$

The friction factor coefficient is computed as:

$$f = \frac{2}{\left(\frac{L}{D_i}\right)} \frac{\Delta P}{\rho U^2} \quad (13)$$

Several correlations and data from the literature were utilized to validate the numerical model's conclusions. To obtain the heat transfer performance in a parabolic trough receiver tube, the friction factor was calculated using the correlation of [36]:

$$f = 0.173\,Re^{-0.1974} \quad (14)$$

The average Nu is expressed as:

$$Nu = \frac{h_f \cdot D_i}{k_f} \quad (15)$$

where k_{eff} is the effective thermal conductivity ($Wm^{-1}K^{-1}$).

$$Nu = \frac{(f/8)(Re - 1.00)\,Pr}{1 + 12.7((f/8)^{0.5}(Pr^{2/3} - 1)} \quad (16)$$

with $Pr \leq 2000$ and $10^3 \leq Re \leq 5 \times 10^6$.

The Reynolds number is given by:

$$Re = \frac{\rho \cdot U \cdot D_i}{\mu} \quad (17)$$

X. BOUNDARY CONDITIONS

For the intake and outlet of the absorber tube, constant mass flow rate, temperature, and outflow boundary conditions were adopted. To generate more realistic findings, a non-uniform heat flow profile around the perimeter of the receiver's absorber tube was examined. SolTrace calculates the solar heat flux density to derive the heat flux distribution profile under direct normal irradiation of $1000W/m^2$. The flux is centered on the lowest half, which is facing the PTC's mirror. The heat flow density is really low in the higher section. In reality, the radiation that comes into contact with the face in this section is direct radiation.

XI. OPTICAL MODELLING (SOLAR HEAT FLUX DENSITY)

For the optical modeling of the collector, SolTrace software was used to predict the effective heat flux falling on the bottom of the absorber tube and to find the effective rays concentrating on the receiver tube using the Monte Carlo ray tracing algorithm. The sun form is characterized by a Gaussian distribution with a standard deviation of 2mrad. Mirror secularity and slope flaws were both taken into account. The efficient rays focused on the outer surface of the absorber tube were discovered using the Monte Carlo ray tracing approach. Figure 4 depicts the distribution of the solar heat flow around the outside wall of the receiving tube. The flux is concentrated on the lower part which is facing the PTC's mirror. For the upper part, the heat flux density is very low (direct solar radiation). Data polynomial functions were created into a macro in Fluent CFD simulation as a User Defined Function (UDF), which is used as the boundary condition input for the heat flux wall on the absorber tube's outer surface as seen in Figure 5. No-slip conditions were applied to all solid surfaces.

(a)

(b)

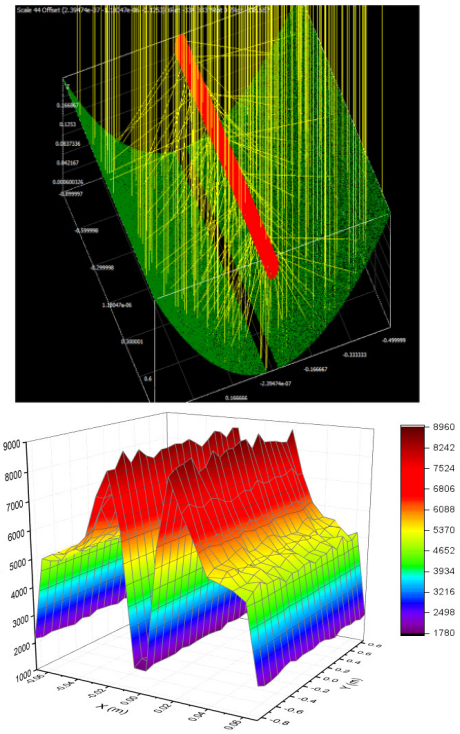

Fig. 4. (a) Ray tracing parabolic reflector and absorber tube surface, (b) 3-dimensional view of the heat flux distribution on the absorber tube surface.

XII. MODEL VALIDATION

To confirm the solution's validity, the precision of the computational modeling was calculated and a comparison with previously reported experimental and theoretical correlations for the local Nusselt variation and pressure drop were performed. The model's validity is evaluated using the experimental data from [38]. The geometry and thermal boundary conditions are nearly identical to those in this simulation.

(a)

(b)

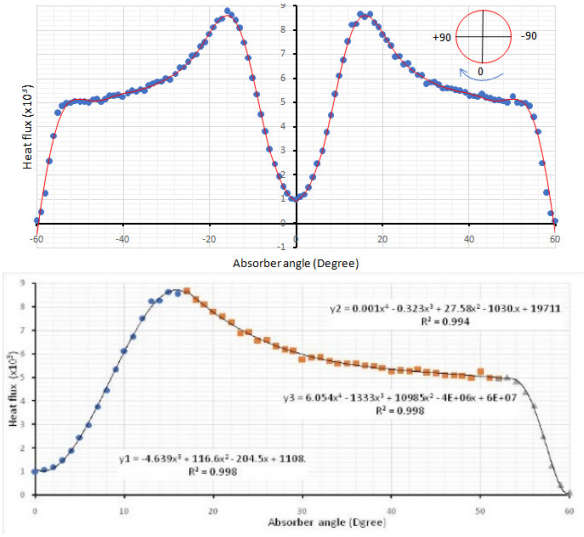

Fig. 5. (a) Circumferential heat flux distribution on the absorber tube. (b) polynomial functions of heat flux profile on the outer surface of the absorber.

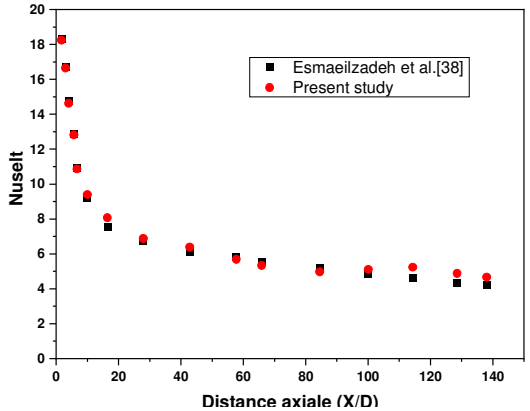

Fig. 6. Comparison of the obtained Nusselt number with [38].

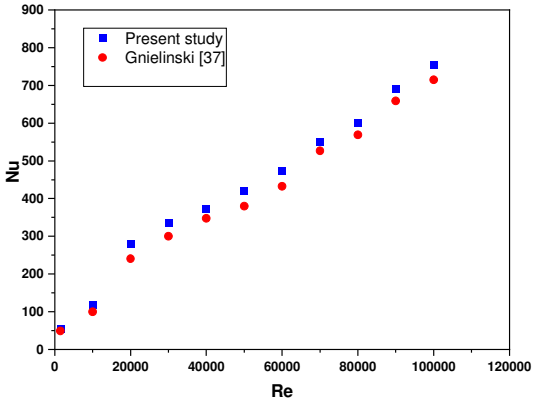

Fig. 7. Comparison of Nu with the result of [37].

The authors in [38] investigated the effect of incorporating Al_2O_3 nanoparticles into pure water on the hydrodynamic and heat transfer parameters of laminar flow at Re = 799.53 inside horizontal flow with uniform heat flux of 9000W/m^2 on the outer pipe wall. According to Figure 6, the current study's modeling results match the experimental results of [38]. Numerical results deviate from experimental data by

approximately 3.5% for the estimation of Nu when φ=1%. Gnielinski correlations were used to validate the results of our numerical study for heat transfer when φ=0% [37] given by (16), As shown in Figure 7, the present study results are shown to be in good agreement with the given correlations. The friction factors were compared with the results from [36], given by (14). Excellent agreement was obtained, as shown in Figure 8, with a deviation of less than 3%. The results indicate that the model and the calculation process are appropriate and acceptable.

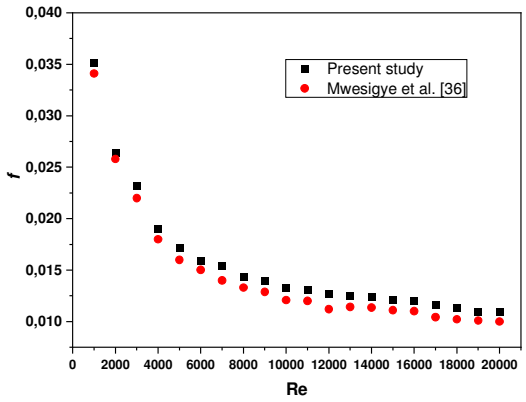

Fig. 8. Validation of present study friction factor with [36] for φ= 4%.

XIII. RESULTS AND DISCUSSION

As a heat flux boundary condition, a UDF was used to connect the acquired heat flux profile to a CFD. Figure 9 depicts the heat flux distribution and temperature distribution on the outer surface of the absorber tube. For typical working condition of HTF inlet mass flow rate, DNI, and HTF inlet temperature of 0.005m/s, 1000W/m^2, and 300K respectively, the performance of the solar collector was tested using water as HTF.

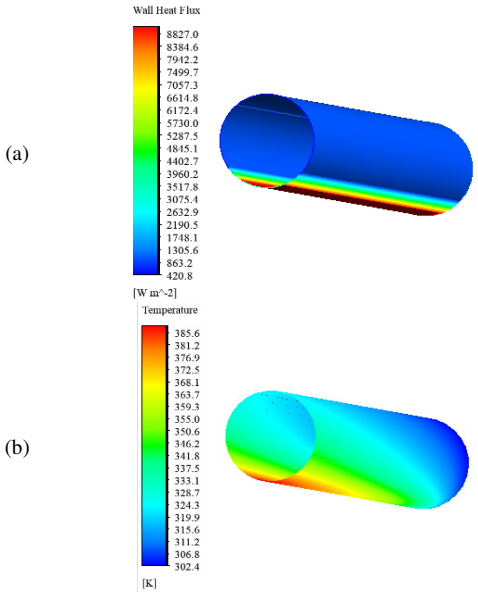

Fig. 9. (a) CFD heat flux, (b) temperature distributions on the outer surface of the absorber tube.

A. *Effect of the Absorber Tube Material*

Figure 10 depicts the temperature distribution on the outside of the absorber tube for various materials. When the thermophysical properties of the absorber vary and the distribution of heat flux on the outer wall changes, the temperature distribution varies over the entire tube wall. Due to its lower thermal conductivity, the steel absorber tube has a poor circumferential temperature distribution. Copper has higher thermal properties than stainless steel, but it has a higher self-weight and lower mechanical strength [3].

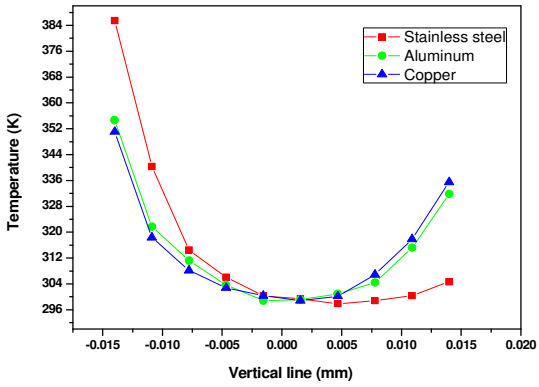

Fig. 10. Distribution of the outlet temperature.

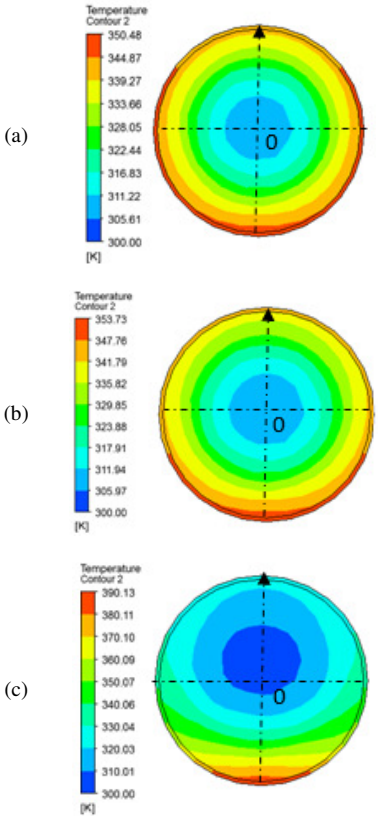

Fig. 11. Temperature variation from bottom wall to top wall of the absorber: (a) Cooper, (b) aluminium, (c) stainless stell.

Figure 11 shows the temperature profiles around the diameter of the inner surface of the absorber tube at the outlet

section. Among the three materials, the temperature of stainless steel is the maximum due to its low thermal conductivity. The temperature gradients with stainless steel are much higher than those of aluminium and copper. The radial temperature distribution is asymmetrical. This can cause higher thermal stresses and reduce the durability of the absorber tube. Circumferential temperature distribution of different absorber tubes is presented in Figure 12 for different absorber tube materials.

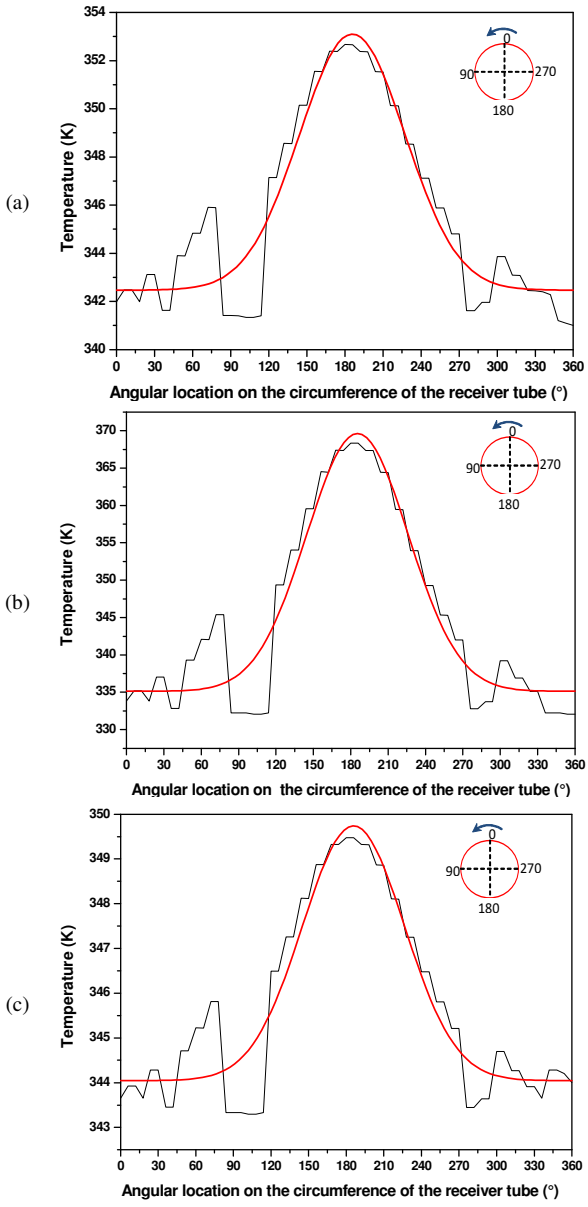

Fig. 12. Circumferential temperature distribution on absorber tube at outlet section (Re=1400): (a) Stainless steel, (b) aluminium, (c) copper.

The temperature distributions changed with angle φ for the three materials. The top wall (φ=0°) temperature remains approximately constant, while for the bottom wall (φ=180°) it is maximum with a very significant gradient. This part of the absorber tube receiver concentrated solar radiation. The stainless-steel has the greatest maximum temperature. The maximum circumferential temperature of stainless steel and aluminium is approximately 10% and 6% higher than the maximum temperature obtained using copper. The temperature gradients of the stainless-steel tube receiver are much greater than those of the aluminium and copper tube receivers. It can be seen that copper has better circumferential temperature distribution than other materials. The circumferential temperature difference (ΔTc) is 34K, 10K, and 6K for stainless steel, aluminium, and copper respectively.

As can be seen in Figure 13, the temperature increases along the length of the tube from the inlet to the outlet. Due to the non-uniform circumferential heat flux distribution, temperature variation in the z direction is negligible compared to the circumferential direction temperature variation. The temperature profiles increase almost linearly and cannot create any stresses. The stress distributions are fully dependent on the wall temperature.

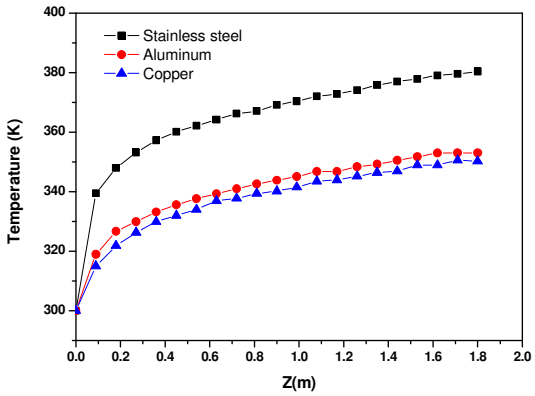

Fig. 13. Axial temperature profiles at the tube inner surface (bottom wall).

B. Thermal Stress Analysis

When the temperature of a continuous body varies in the presence of constraints, thermal stress can arise. In the present study, thermal stress analysis was conducted along the heat transfer fluid's current. The static structural module of ANSYS was used. The thermal stress of the tubes in the thermoelastic model is totally determined by the temperature profiles. The temperature data from the tubes obtained from the thermal model could be used as the boundary conditions in the thermoelastic model's nodes. In addition, the material tube was supposed to be isotropic and elastically deformed under temperature load. The stress levels and distributions are determined by the combined effects of circumferential axial and radial temperature gradients on the PTC receiver tube.

Figure 14 shows the axial stress profiles for the three different materials on the inner surface tube along the length direction at bottom wall. Stainless steel axial compressive stress values are significantly higher than the ones of aluminium and copper. The axial stress values of all materials are close to zero at the inlet and outlet ends, and they increase rapidly to higher values that are close to the profile's peak compressive axial stress values. The temperature profiles along the axial direction at the tube inner surface illustrated in Figure 13 can explain these phenomena. As can be seen from this Figure, the temperature profiles at the tree tube receiver ends

increase almost linearly along the axial direction, which cannot create any stresses and the stress distributions are fully dependent on the wall temperature. Figure 15 shows the radial stress profiles on the inner surface tube along the axial direction for the different material conditions at bottom wall. The radial stresses act as tensile stress at the tube outlet and inlet ends for all the tree material, and then the radial stress values suddenly change to compressive stress. The radial stress values are approximately constant from z = 0.1 m to z = 1.7 m, which is near to zero. The highest maximum radial stress is 3.2 MPa in stainless steel. The maximum radial stress for aluminium and copper conditions is very small, at about 1.6 MPa and 0.6 MPa, respectively.

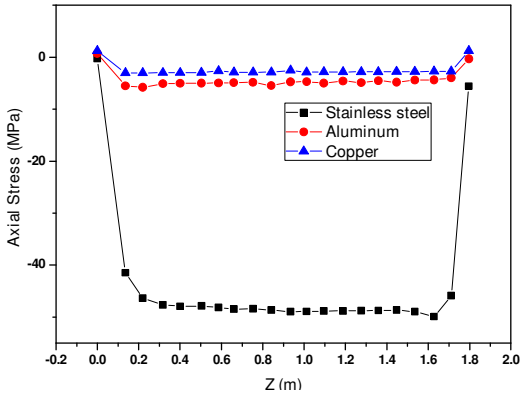

Fig. 14. Axial stress profiles on the inner surface tube along the length direction at bottom wall.

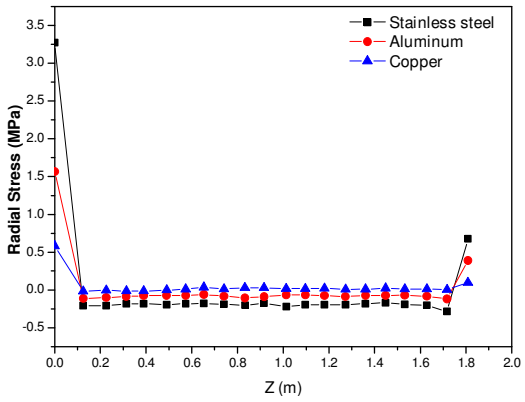

Fig. 15. Radial stress profiles on the inner surface tube at bottom wall.

As can be seen in Figure 16, the circumferential stress of the absorber tube is greatest at a circumference angle of the bottom wall because the temperature there is the highest hence the stress created in this area is the greatest. As the temperature drops, the circumferential stress decreases. The circumferential stress is lower at the top surface of the absorber tube, where the temperature is lower. On the other hand, the temperature difference between the local temperatures of the wall and the fluid influences local heat transfer from the wall, resulting in greater strain at the tube's bottom. Maximum stress is found in stainless steel and the lowest stress in copper.

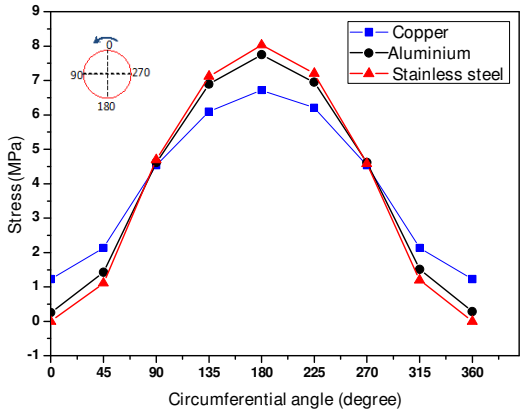

Fig. 16. Circumferential stress distribution of the absorber tube.

C. *Effect of the Al_2O_3 Concentration*

A numerical simulation with three different volumetric concentrations of Al_2O_3, equal to 2%, 4%, and 6%, is used to investigate the influence of Al_2O_3 volume fraction on the performance of the solar receiver when the mass flowrate of the HTF is 5g/s. In order to investigate the solar receiver's performance, a non-uniform solar radiation heat flux distribution on the outer wall of the absorber tube is used as a boundary condition. Figures 17 and 18 depict the effects of Al_2O_3 volume fractions on the temperature distributions of the absorber wall with nanoparticle volume fractions ranging from 0% to 6%.

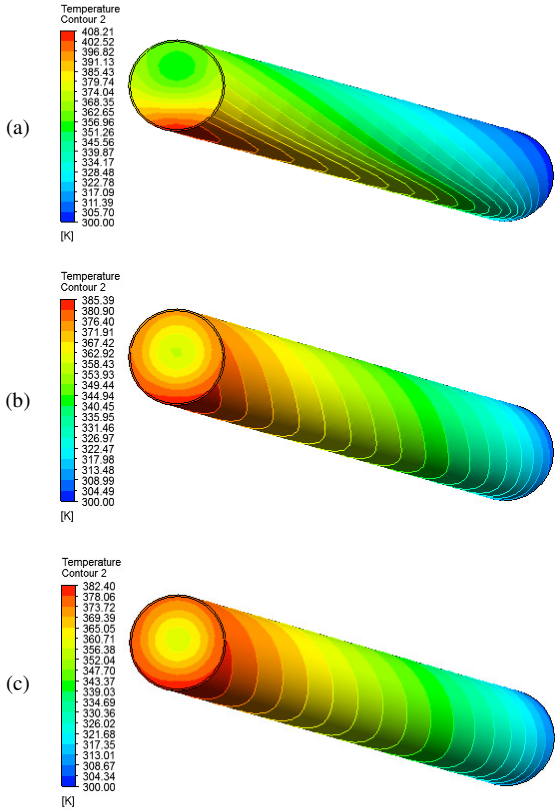

Fig. 17. Temperature distribution vs. nanoparticle concentration (Re=1300): (a) φ=1%, (b) φ=2%, (c) φ=6%.

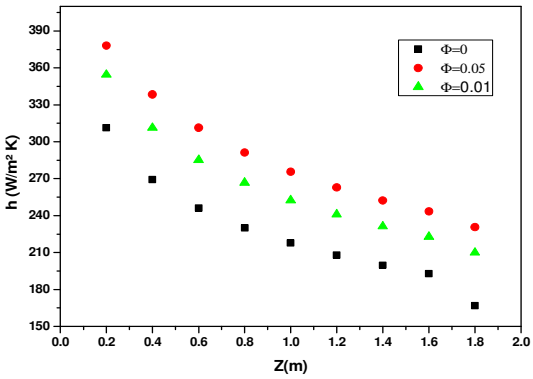

Fig. 18. Average and maximum temperature distribution of the absorber wall under different volume fractions of Al_2O_3 (Re=1300).

According to these findings, the average and maximum temperatures of the absorber tube fall noticeably as the volume fraction increases. As the volume percentages of Al_2O_3 grow from 0% to 6%, the maximum temperature drops from 408.4K to 382K. As a result, the thermal gradients in the absorber tube and the receiver's heat loss are decreased.

Figure 19 shows the axial variation of the local Nusselt number for different volume fractions of Al_2O_3 nanoparticles. From the results, it is clear that the addition of nanoparticles to the base fluid has a direct effect in the field of heat transfer. In these conditions, the Nusselt number of the nanofluid is greater than that of pure water. It increases significantly with an increasing volume concentration of nanoparticles. So, it is confirmed that the suspension of nanoparticles in its base fluid gives a remarkable increase in heat exchange.

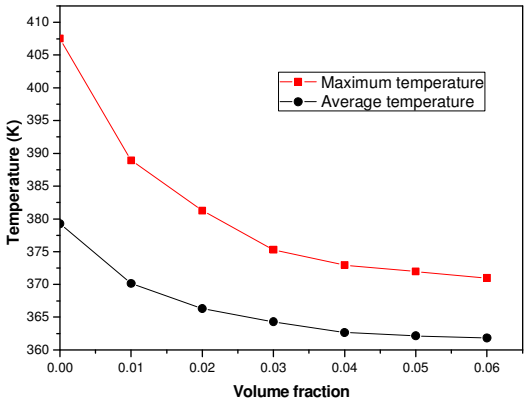

Fig. 19. Variation of local Nusselt number (Re=1300).

Figure 20 illustrates the axial variation of the convection heat transfer coefficients along the axial direction of the absorber tube for Re=1300 and different volume concentrations of nanoparticles. It is obvious that the convection heat transfer coefficient increases as the volume fraction of the nanoparticles increases. The main reason is that when the volume percentage of nanoparticles increases, the thermophysical properties of the fluid improve.

Figure 21 shows the axial temperature variation for different Al_2O_3 nanoparticle volume fraction. It is clear that the growth in the shape of the curves is due to the increase in the volume fraction of the Al_2O_3 nanoparticles, due to their effective thermal conductivity, which is higher than water's. This generates an increase in the exchange coefficient h and in the temperature values. At outlet (Z=1.8m), the temperature reaches T=318K for φ=6% and T=310K for φ=0%.

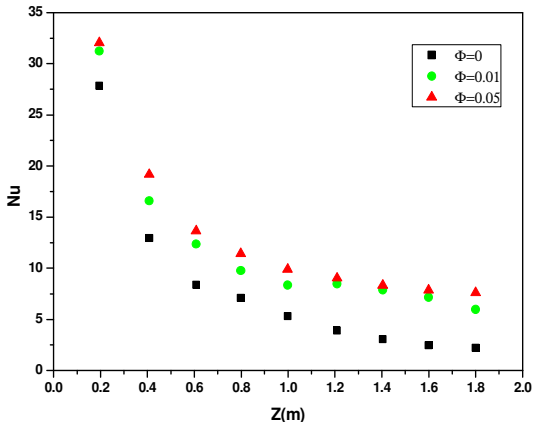

Fig. 20. Variation of the heat transfer coefficients (Re=1300).

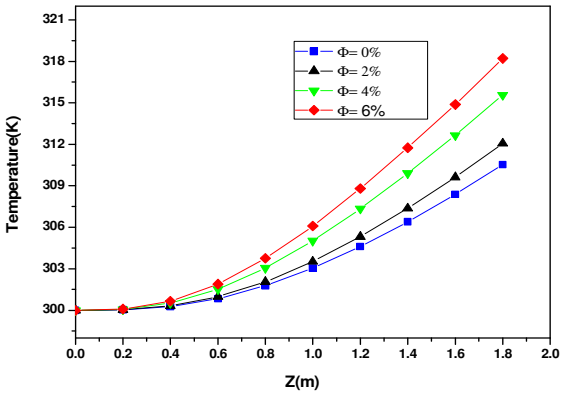

Fig. 21. Axial temperature for different volume fractions of Al_2O_3.

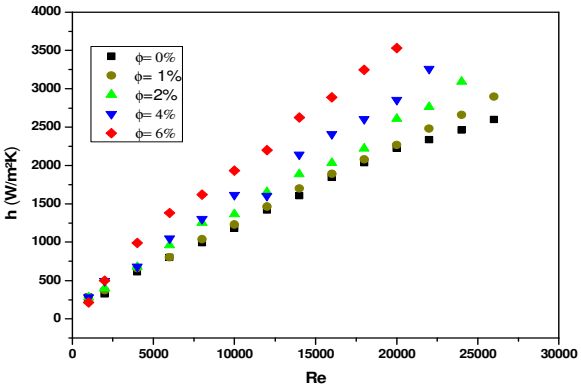

Fig. 22. Heat transfer coefficient vs. nanoparticle volume fraction and Reynolds number for Tinl=300K.

Figure 22 shows the heat transfer coefficient as a function of Re and nanoparticle volume fraction at inlet temperature T_{inl}=300K. As shown in the Figure, using nanofluids improves heat transfer performance when compared to the base fluid (φ= 0%). It can be seen that the heat transfer coefficient

increases by 48%, 38%, and 33% as the volume fraction increases by 8%, 6%, and 4% respectively, especially at higher Reynolds number values. As a result, the improvement in heat transfer performance must be greater than the increase in pump capacity for the usage of nanofluids to be economically viable.

It is vital to understand pressure drop in order to build the best pump available. The pressure drop is also explored in this work. The pressure drop between the collector's intake and output ports was determined using the simulation data. Figure 23 shows that when the volume fraction grows, the pressure drop increases dramatically, especially at higher Reynolds numbers. When the particle volumetric concentration in the nanofluid increases, the density and viscosity rise, causing an increase in pressure drop. This increases flow resistance and necessitates more pumping power. This causes an increase in flow resistance and needs additional pumping force.

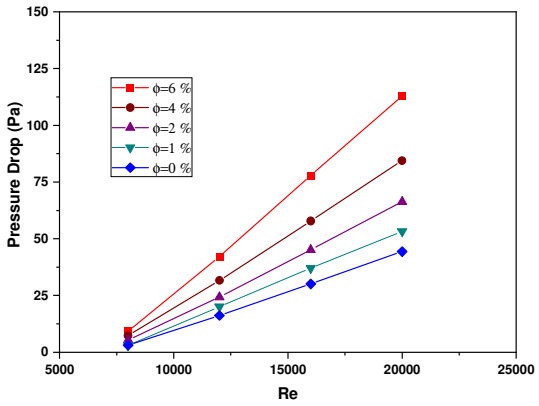

Fig. 23. Pressure drop in the absorber tube vs. nanoparticle volume fraction and Reynolds number.

Figure 24 shows the change in the velocity profile. The profile is tested at axial locations z = 0, 0.1, 0.6, 1.2, 1.80m and for volume concentrations of 1%, 2%, and 6%. The velocity of the working fluid is constant at the inlet. From this section and beyond the velocity increases, and the profile becomes less flattened. The maximum velocity is not reached at the center, and it is pushed down, due to the fact that the fluid is heated asymmetrically because the solar heat flux distribution is not uniform. There is an angle towards the end of the entering area. An increase in particle volume fraction is, therefore, advantageous in terms of energy utilization. A higher temperature rise of the nanofluid will lead to higher collector thermal efficiency. However, increased particle loading also increases fluid viscosity, which affects pressure drop.

According to Figure 25, the collector's efficiency decreases considerably as the volume fraction increases due to the nanofluid's increased heat conductivity. The thermal efficiency decreases continually as Re increases. Pressure drop increases significantly at much higher Re values, therefore, the increase in pumping power outweighs by far the gain in thermal performance, leading to lower efficiency. It is concluded that for nanoparticle volume fractions ranging from 2 to 6%, thermal efficiency increases by 3 to 14%.

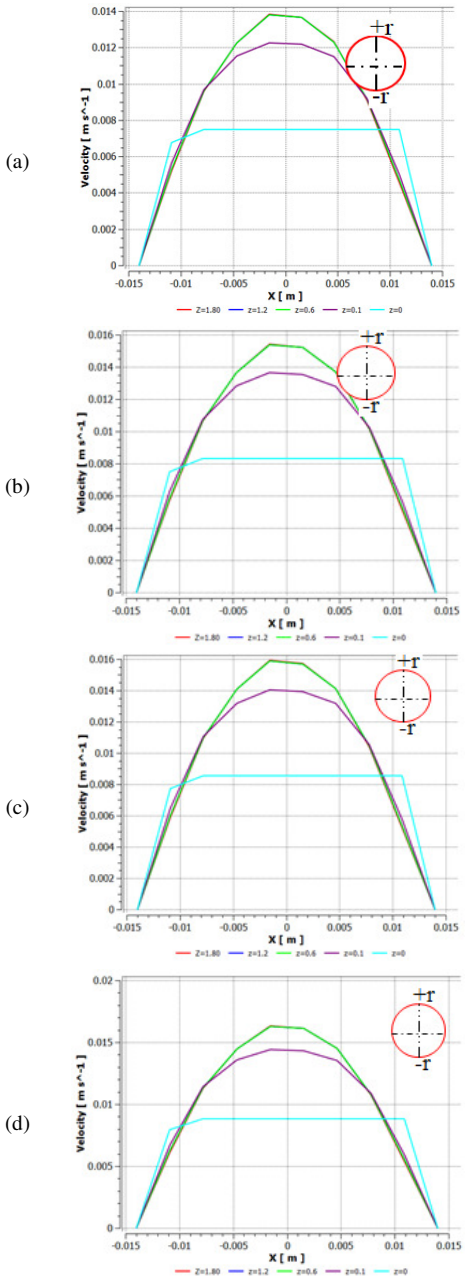

Fig. 24. Velocity profiles for (a) φ=6%, (b) φ=4%, (c) φ=2%, (d) φ=0%.

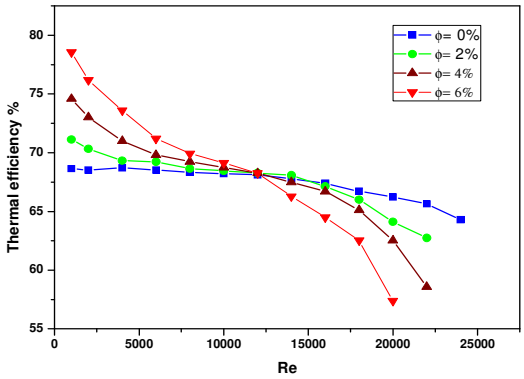

Fig. 25. Thermal efficiency vs. volume fraction and Re for Tinl=300K.

XIV. CONCLUSION

In this paper, 3-dimensional numerical simulation of a PTC system under solar NUHF on the outer surface of the absorber tube were used to evaluate the influence of material selection on the thermal and the thermal stresses of tube receivers. Moreover, the use of Al_2O_3/water nanofluid as HTF was proposed to improve the performances of the PTC system. This study is a preliminary overview of the key parameters which promote the optimization of the absorber tube by homogenizing heat flux distribution, reducing peak temperature and decreasing the temperature gradient to reduce thermal stresses, which are generated by the high temperature gradients. Three materials (copper, stainless steel, and aluminum) and nanoparticles of Al_2O_3 with concentration ratios ranging from 0% to 6 % were used. The results confirmed that:

- Receiver tube material selection is critical for ensuring reliability. The temperature gradients with stainless steel are much higher than those with aluminum and copper gradients, which can cause higher thermal stresses and reduces durability of the absorber tube.
- The maximum circumferential temperature of stainless steel and aluminium is approximately 10% and 6% higher than the maximum temperature obtained using copper. The temperature gradient of the stainless-steel tube receivers is much greater than those of the aluminum and copper tube receivers. Copper has a better circumferential temperature distribution than the other materials. For stainless steel, aluminium, and copper, the circumferential temperature difference (ΔT) is 34K, 10K, and 6K respectively. Copper is the recommended material as the receiver tube material from the point of view of thermal stress.
- The temperature gradient and the maximum temperature in the absorber are greatly reduced by using Al_2O_3/water as HTF. The temperature gradient and the maximum temperature in the absorber decrease with the Al_2O_3 particle concentration.
- Increase in nanoparticle volume fraction by 1%, 2%, and 6% increases the average of output temperatures by 2%, 6%, and 10% respectively.
- Heat transfer coefficient increases by 48%, 38% and 33% as the volume fraction increases to 8%, 6%, and 4% respectively, especially at higher Reynolds numbers. The study concluded that for nanoparticle volume fractions ranging from 2% to 6%, thermal efficiency increases by 3% to-14%.

In future work, the study will be focused towards the effect of other receiver tube material and the results will be used for the design and manufacturing of a more efficient parabolic trough solar receiver.

REFERENCES

[1] N. B. Khedher, "Experimental Evaluation of a Flat Plate Solar Collector Under Hail City Climate," *Engineering, Technology & Applied Science Research*, vol. 8, no. 2, pp. 2750–2754, Apr. 2018, https://doi.org/10.48084/etasr.1957.

[2] R. Almanza, A. Lentz, and G. Jimenez, "Receiver behavior in direct steam generation with parabolic troughs," *Solar Energy*, vol. 61, no. 4, pp. 275–278, Oct. 1997, https://doi.org/10.1016/S0038-092X(97)88854-8.

[3] H. Price *et al.*, "Advances in Parabolic Trough Solar Power Technology," *Journal of Solar Energy Engineering*, vol. 124, no. 2, pp. 109–125, Apr. 2002, https://doi.org/10.1115/1.1467922.

[4] M. A. Irfan and W. Chapman, "Thermal stresses in radiant tubes due to axial, circumferential and radial temperature distributions," *Applied Thermal Engineering*, vol. 29, no. 10, pp. 1913–1920, Jul. 2009, https://doi.org/10.1016/j.applthermaleng.2008.08.021.

[5] P. Wang, D. Y. Liu, and C. Xu, "Numerical study of heat transfer enhancement in the receiver tube of direct steam generation with parabolic trough by inserting metal foams," *Applied Energy*, vol. 102, pp. 449–460, Feb. 2013, https://doi.org/10.1016/j.apenergy.2012.07.026.

[6] Y.-L. He, K. Wang, Y. Qiu, B.-C. Du, Q. Liang, and S. Du, "Review of the solar flux distribution in concentrated solar power: Non-uniform features, challenges, and solutions," *Applied Thermal Engineering*, vol. 149, pp. 448–474, Feb. 2019, https://doi.org/10.1016/j.applthermaleng.2018.12.006.

[7] S. Khanna, V. Sharma, S. Singh, and S. B. Kedare, "Explicit expression for temperature distribution of receiver of parabolic trough concentrator considering bimetallic absorber tube," *Applied Thermal Engineering*, vol. 103, pp. 323–332, Jun. 2016, https://doi.org/10.1016/j.applthermaleng.2016.04.110.

[8] W. Fuqiang, T. Zhexiang, G. Xiangtao, T. Jianyu, H. Huaizhi, and L. Bingxi, "Heat transfer performance enhancement and thermal strain restrain of tube receiver for parabolic trough solar collector by using asymmetric outward convex corrugated tube," *Energy*, vol. 114, pp. 275–292, Nov. 2016, https://doi.org/10.1016/j.energy.2016.08.013.

[9] Y. Aldali, T. Muneer, and D. Henderson, "Solar absorber tube analysis: thermal simulation using CFD," *International Journal of Low-Carbon Technologies*, vol. 8, no. 1, pp. 14–19, Mar. 2013, https://doi.org/10.1093/ijlct/ctr039.

[10] M. R. Haddouche and A. Benazza, "Numerical Investigation and Solar Flux Distribution Analysis of Parabolic Trough Solar Collector by Adding Secondary Reflector," *Instrumentation Mesure Metrologie*, vol. 18, pp. 275–280, Aug. 2019, https://doi.org/10.18280/i2m.180307.

[11] C.-Y. Tsai and P. D. Lin, "Optimized variable-focus-parabolic-trough reflector for solar thermal concentrator system," *Solar Energy*, vol. 86, no. 5, pp. 1164–1172, May 2012, https://doi.org/10.1016/j.solener.2012.01.009.

[12] E. Bellos and C. Tzivanidis, "Investigation of a booster secondary reflector for a parabolic trough solar collector," *Solar Energy*, vol. 179, pp. 174–185, Feb. 2019, https://doi.org/10.1016/j.solener.2018.12.071.

[13] Z. Wu, S. Li, G. Yuan, D. Lei, and Z. Wang, "Three-dimensional numerical study of heat transfer characteristics of parabolic trough receiver," *Applied Energy*, vol. 113, pp. 902–911, Jan. 2014, https://doi.org/10.1016/j.apenergy.2013.07.050.

[14] R. Senthil, C. Rath, and M. Gupta, "Enhancement of uniform temperature distribution on the concentrated solar receiver with integrated phase change material," *International Journal of Mechanical Engineering and Technology*, vol. 8, no. 9, pp. 315–320, Sep. 2017.

[15] D. Guerraiche, C. Bougriou, K. Guerraiche, L. Valenzuela, and Z. Driss, "Experimental and numerical study of a solar collector using phase change material as heat storage," *Journal of Energy Storage*, vol. 27, Feb. 2020, Art. no. 101133, https://doi.org/10.1016/j.est.2019.101133.

[16] P. Liu, Z. Dong, H. Xiao, Z. Liu, and W. Liu, "Thermal-hydraulic performance analysis of a novel parabolic trough receiver with double tube for solar cascade heat collection," *Energy*, vol. 219, Mar. 2021, Art. no. 119566, https://doi.org/10.1016/j.energy.2020.119566.

[17] M. Keshavarz Moraveji and S. Razvarz, "Experimental investigation of aluminum oxide nanofluid on heat pipe thermal performance," *International Communications in Heat and Mass Transfer*, vol. 39, no. 9, pp. 1444–1448, Nov. 2012, https://doi.org/10.1016/j.icheatmasstransfer.2012.07.024.

[18] N. Abed, I. Afgan, H. Iacovides, A. Cioncolini, I. Khurshid, and A. Nasser, "Thermal-Hydraulic Analysis of Parabolic Trough Collectors

Using Straight Conical Strip Inserts with Nanofluids," *Nanomaterials*, vol. 11, no. 4, Apr. 2021, Art. no. 853, https://doi.org/10.3390/nano11040853.

[19] H. A. Fakhim, "An Investigation of the Effect of Different Nanofluids in a Solar Collector," *Engineering, Technology & Applied Science Research*, vol. 7, no. 4, pp. 1741–1745, Aug. 2017, https://doi.org/10.48084/etasr.1283.

[20] H. B. Lanjwani, M. S. Chandio, K. Malik, and M. M. Shaikh, "Stability Analysis of Boundary Layer Flow and Heat Transfer of Fe2O3 and Fe-Water Base Nanofluid over a Stretching/Shrinking Sheet with Radiation Effect," *Engineering, Technology & Applied Science Research*, vol. 12, no. 1, pp. 8114–8122, Feb. 2022, https://doi.org/10.48084/etasr.4649.

[21] K. Boukerma and M. Kadja, "Convective Heat Transfer of Al2O3 and CuO Nanofluids Using Various Mixtures of Water-Ethylene Glycol as Base Fluids," *Engineering, Technology & Applied Science Research*, vol. 7, no. 2, pp. 1496–1503, Apr. 2017, https://doi.org/10.48084/etasr.1051.

[22] T. P. Otanicar, P. E. Phelan, R. S. Prasher, G. Rosengarten, and R. A. Taylor, "Nanofluid-based direct absorption solar collector," *Journal of Renewable and Sustainable Energy*, vol. 2, no. 3, May 2010, Art. no. 033102, https://doi.org/10.1063/1.3429737.

[23] S. Hassani, R. Saidur, S. Mekhilef, and A. Hepbasli, "A new correlation for predicting the thermal conductivity of nanofluids; using dimensional analysis," *International Journal of Heat and Mass Transfer*, vol. 90, pp. 121–130, Nov. 2015, https://doi.org/10.1016/j.ijheatmasstransfer.2015.06.040.

[24] V. Verma and L. Kundan, "Thermal Performance Evaluation of a Direct Absorption Flat Plate Solar Collector (DASC) using Al2O3-H2O Based Nanofluids," *IOSR Journal of Mechanical and Civil Engineering*, vol. 6, no. 2, pp. 29–35, 2013.

[25] D. R. Waghole, R. M. Warkhedkar, V. S. Kulkarni, and R. K. Shrivastva, "Experimental Investigations on Heat Transfer and Friction Factor of Silver Nanofliud in Absorber/Receiver of Parabolic Trough Collector with Twisted Tape Inserts," *Energy Procedia*, vol. 45, pp. 558–567, Jan. 2014, https://doi.org/10.1016/j.egypro.2014.01.060.

[26] R. A. Taylor *et al.*, "Applicability of nanofluids in high flux solar collectors," *Journal of Renewable and Sustainable Energy*, vol. 3, no. 2, Mar. 2011, Art. no. 023104, https://doi.org/10.1063/1.3571565.

[27] T. Sokhansefat, A. B. Kasaeian, and F. Kowsary, "Heat transfer enhancement in parabolic trough collector tube using Al2O3/synthetic oil nanofluid," *Renewable and Sustainable Energy Reviews*, vol. 33, pp. 636–644, May 2014, https://doi.org/10.1016/j.rser.2014.02.028.

[28] T. Yousefi, F. Veysi, E. Shojaeizadeh, and S. Zinadini, "An experimental investigation on the effect of Al2O3–H2O nanofluid on the efficiency of flat-plate solar collectors," *Renewable Energy*, vol. 39, no. 1, pp. 293–298, Mar. 2012, https://doi.org/10.1016/j.renene.2011.08.056.

[29] M. Mahmoodi and S. M. Hashemi, "Numerical study of natural convection of a nanofluid in C-shaped enclosures," *International Journal of Thermal Sciences*, vol. 55, pp. 76–89, May 2012, https://doi.org/10.1016/j.ijthermalsci.2012.01.002.

[30] R. Forristall, "Heat Transfer Analysis and Modeling of a Parabolic Trough Solar Receiver Implemented in Engineering Equation Solver," National Renewable Energy Lab, Golden, CO, United States, NREL/TP-550-34169, Oct. 2003. https://doi.org/10.2172/15004820.

[31] Y. Wang, Q. Liu, J. Lei, and H. Jin, "Performance analysis of a parabolic trough solar collector with non-uniform solar flux conditions," *International Journal of Heat and Mass Transfer*, vol. 82, pp. 236–249, Mar. 2015, https://doi.org/10.1016/j.ijheatmasstransfer.2014.11.055.

[32] S. El Becaye Maiga, C. Tam Nguyen, N. Galanis, G. Roy, T. Mare, and M. Coqueux, "Heat transfer enhancement in turbulent tube flow using Al2O3 nanoparticle suspension," *International Journal of Numerical Methods for Heat & Fluid Flow*, vol. 16, no. 3, pp. 275–292, Jan. 2006, https://doi.org/10.1108/09615530610649717.

[33] R. Ekiciler, K. Arslan, O. Turgut, and B. Kursun, "Effect of hybrid nanofluid on heat transfer performance of parabolic trough solar collector receiver," *Journal of Thermal Analysis and Calorimetry*, vol. 143, no. 2, pp. 1637–1654, Jan. 2021, https://doi.org/10.1007/s10973-020-09717-5.

[34] K. Wang, Y. He, and Z. Cheng, "A design method and numerical study for a new type parabolic trough solar collector with uniform solar flux distribution," *Science China Technological Sciences*, vol. 57, no. 3, pp. 531–540, Mar. 2014, https://doi.org/10.1007/s11431-013-5452-6.

[35] M. S. Bretado de los Rios, C. I. Rivera-Solorio, and A. J. Garcia-Cuellar, "Thermal performance of a parabolic trough linear collector using Al2O3/H2O nanofluids," *Renewable Energy*, vol. 122, pp. 665–673, Jul. 2018, https://doi.org/10.1016/j.renene.2018.01.094.

[36] A. Mwesigye, T. Bello-Ochende, and J. P. Meyer, "Heat transfer and thermodynamic performance of a parabolic trough receiver with centrally placed perforated plate inserts," *Applied Energy*, vol. 136, pp. 989–1003, Dec. 2014, https://doi.org/10.1016/j.apenergy.2014.03.037.

[37] V. Gnielinski, "On heat transfer in tubes," *International Journal of Heat and Mass Transfer*, vol. 63, pp. 134–140, Aug. 2013, https://doi.org/10.1016/j.ijheatmasstransfer.2013.04.015.

[38] E. Esmaeilzadeh, H. Almohammadi, Sh. Nasiri Vatan, and A. N. Omrani, "Experimental investigation of hydrodynamics and heat transfer characteristics of γ-Al2O3/water under laminar flow inside a horizontal tube," *International Journal of Thermal Sciences*, vol. 63, pp. 31–37, Jan. 2013, https://doi.org/10.1016/j.ijthermalsci.2012.07.001.